

An Objective Climatology of Carolina Coastal Fronts

K. WYAT APPEL

U.S. Environmental Protection Agency, Research Triangle Park, North Carolina

ALLEN J. RIORDAN

North Carolina State University, Raleigh, North Carolina

TIMOTHY A. HOLLEY

Weathernews Americas, Inc., Norman, Oklahoma

(Manuscript received 15 June 2004, in final form 1 February 2005)

ABSTRACT

This study describes a simple objective method to identify cases of coastal frontogenesis offshore of the Carolinas and to characterize the sensible weather associated with frontal passage at measurement sites near the coast. The identification method, based on surface hourly data from offshore and adjacent land stations, was applied to an 11-yr dataset (1984–94). A total of 379 coastal fronts was found, 70 of which eventually made landfall along the North Carolina coast; 112 that remained offshore, and 197 were termed diurnal since they remained offshore but disappeared during daylight hours.

Results show that most coastal and offshore sites experience a wind shift of about 40°–70° and a warming of about 2°–3°C during the hour of frontal passage. Exceptions include sites near colder waters where the rates are markedly reduced and frontal passage is often less discernible. Excluding diurnal fronts, just over half the cases were associated with cold-air damming (CAD) during the cold season of 16 October–15 April. Most of these winter cases linked with CAD were onshore fronts. During the warm season, most fronts were diurnal, but the association with CAD was still significant.

To explore the synoptic-scale environment, composite maps for the cold season were generated for all three frontal subtypes from NCEP–NCAR reanalysis data. Results show a strong surface anticyclone centered north of the region of frontogenesis for all three composites. However, several features in the synoptic-scale regimes appear to differentiate the three frontal types. For example, cyclogenesis in the Gulf of Mexico and onshore southeasterly low-level flow along the southeast Atlantic coast accompanied by warm advection distinguish onshore fronts from the other two types. The offshore fronts are accompanied by more nearly zonal flow aloft and a surface anticyclone that stalls near the New England coastline. Finally, the diurnal type is associated with much weaker pressure and height fields and an east–west elongated surface anticyclone centered much farther south than in the other cases.

1. Introduction

A coastal front is a mesoscale feature that forms in geographically favored areas, such as along the New England and southeast coasts of the United States (Bosart et al. 1972; Nielsen 1989). The latter is a common location for coastal frontogenesis because of the presence of the Appalachian Mountains to the west and the Gulf Stream to the east. During synoptic regimes when high pressure at the surface dominates the north-

east United States, the Gulf Stream provides a source of heat and moisture while the mountains facilitate the southward advance of cold air creating a natural baroclinic zone near the coast.

Coastal fronts in the Southeast generally form during the winter months and are believed to be typically associated with cold-air damming (CAD; Doyle and Warner 1993a). In structure, they resemble shallow quasi-stationary or warm fronts with temperature contrasts that can reach more than 10°C over short distances on the order of 100 km or less (Bosart 1975). Coastal fronts are of major importance in the coastal zone and adjacent inland areas since they are often associated with enhanced cloudiness and precipitation, can mark the transition zone between frozen and liquid

Corresponding author address: Allen J. Riordan, Dept. of Marine, Earth and Atmospheric Sciences, North Carolina State University, Box 8208, Raleigh, NC 27695-8208.
E-mail: al_riordan@ncsu.edu

precipitation, and provide a source of surface convergence and vorticity that often focuses cyclogenesis (Austin 1941; Carson 1950; Marks and Austin 1979; Bosart 1981). When these fronts move ashore, they have sometimes been associated with the development of severe weather (Businger et al. 1991; Vescio et al. 1993).

The cold air on the landward side of the front is often shallow—typically the top of the frontal inversion is less than 1 km from the surface (Carson 1950; Marks and Austin 1979; Nielsen and Neille 1990; Riordan 1990; Raman et al. 1998). Thus, a nearshore coastal front is especially sensitive to turbulent mixing and differential diabatic effects of latent heating and sensible heat transfer from the surface. The latter two effects were shown by Ballentine (1980) to be important in coastal frontogenesis in New England. Consequently the landward movement of coastal fronts is sometimes rapid and discontinuous and is not well depicted by numerical forecast models. For example, a common error in the Eta Model is to forecast premature CAD erosion and inland progression of the coastal front. Such errors in predicting frontal location often translate into 2-m temperature errors of 10°C or more, especially in the coastal zone of the Carolinas. Here a forecast of partly cloudy skies with a temperature of 18°C and southeast winds may contrast sharply with the reality of fog and drizzle with a temperature of 8°C and northeast winds.

Thus, accurate prediction of the onshore movement of coastal fronts is both important and difficult. In fact, a recent informal survey of National Weather Service (NWS) forecasters at coastal stations from Virginia to South Carolina indicated that predicting the sensible weather with coastal fronts ranks as a leading winter forecast challenge.

To provide guidance to regional forecasters, this paper describes a method that may prove useful in predicting the character and behavior of coastal fronts near the North Carolina coastline. First a simple objective algorithm is described for detecting coastal fronts that form offshore of the Carolinas. Through this algorithm, cases are identified in a historical database and classified by their subsequent behavior. Hourly trends in sensible weather that accompany frontal passage are then compared for selected coastal and offshore stations. Finally, for each of the frontal classifications, composite maps are constructed to characterize the synoptic-scale environment common to all and to find features that differentiate each class from the others.

2. Data and methodology

To perform the desired coastal front detection and cataloging, routine hourly surface observations from in

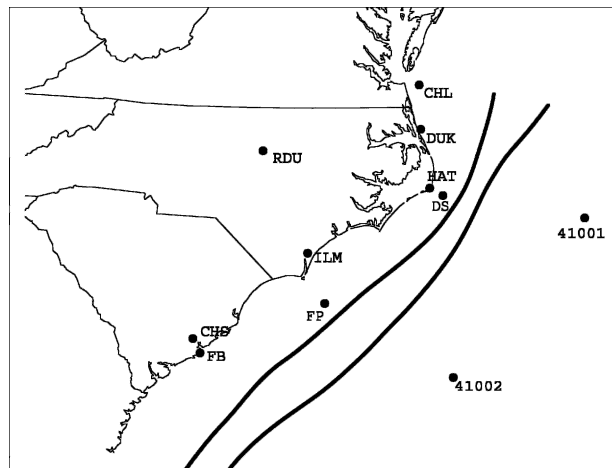


FIG. 1. Sites used in this study including Raleigh–Durham (RDU), Cape Henry Light Tower (CHL), Duck Pier (DUK), buoy 41001, Cape Hatteras (HAT), Diamond Shoals Light Tower (DS), Wilmington (ILM), Frying Pan Shoals Light Tower (FP), Charleston (CHS), Folley Beach (FB), and buoy 41002. Heavy lines depict the normal range of locations of the west edge of the Gulf Stream.

situ offshore and onshore sites were compared. It would have been desirable to include upper-air observations in this comparison, but temporal resolution is insufficient for this purpose. To obtain a large sample of coastal fronts, a sufficiently long and continuous series of hourly data from coastal and offshore platforms was needed. For land stations, datasets derived from the Solar and Meteorological Observation Network (SAMSON) were used. This record is available from the National Climatic Data Center. The National Data Buoy Center (NDBC) maintains a suite of instrumented platforms including Coastal-Marine Automated Network (C-MAN) and moored buoys that served as potential sites. Of the platforms near the southeast coast of the United States, site location and completeness of the data record were the primary criteria for use in this study. Buoys 41001 (34.68°N, 72.23°W) located 280 km east of Cape Hatteras, North Carolina, and 41002 (32.27°N, 75.20°W) located 460 km east of Charleston, South Carolina, met our needs for a large continuous time series of hourly observations (Fig. 1). Data from these moored buoys were obtained from the NDBC archive (at the Web site <http://www.ndbc.noaa.gov>). For reference, the boundaries of the location of the west (cold) wall of the Gulf Stream are also indicated in Fig. 1. These boundaries represent one standard deviation from the mean cold wall position based on a 5-yr study by Olson et al. (1983).

Since coastal fronts generally are accompanied by easterly flow over the ocean and more northerly flow

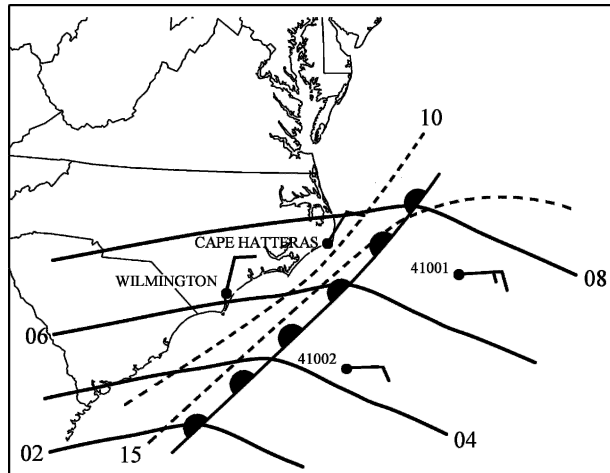


FIG. 2. Schematic representation of a coastal front including sea level pressure (hPa, solid), isotherms ($^{\circ}\text{C}$, dashed), and wind reports at key stations.

over land (Bosart 1975; Riordan 1990), criteria for wind speed and direction were specified in the detection algorithm. A typical scenario is illustrated in Fig. 2 that shows the inverted pressure trough, wind shift, and thermal gradient characteristic of a coastal front. Even though air temperatures at offshore sites in winter are typically warmer than those inland, a threshold value of land – buoy temperature difference was nevertheless specified such that the thermal gradient was consistent with frontal structure.

In the mid-Atlantic region, coastal fronts differ from synoptic-scale cold fronts that move across the inland region from the west and become stationary offshore. Such fronts are typically traceable from the central United States and often are accompanied by a southerly wind set. In other words, winds east of the front are often from the southeast or south while winds immediately behind the front are generally southwest or west. Such a wind regime results from the synoptic-scale cyclone passing to the north. By contrast, coastal fronts form offshore and are accompanied by a northerly wind set, that is, winds from the northeast ahead of the front, and east in the warm air behind the front. Such a regime results from a surface pressure trough that is inverted from that of the typical cold front.

Observational studies and related numerical simulations have shown that coastal frontogenesis typically occurs between the coast and the National Oceanic and Atmospheric Administration (NOAA) offshore buoys 41001 and 41002 (Doyle and Warner 1990, 1993a,b; Riordan 1990; Riordan et al. 1995; Raman et al. 1998). Therefore, data from each buoy were compared with those from the nearest land station. Specifically, buoy

41001 data were compared with the National Weather Service (NWS) measurement site at Cape Hatteras, North Carolina (HAT), and buoy 41002 with the site at Wilmington, North Carolina (ILM).

A two-stage process was developed to detect offshore coastal fronts. The first was based on the conceptual model of Fig. 2. Its primary purpose was to ensure that coastal fronts were detected in favor of synoptic-scale cold fronts. A potential coastal front was identified between HAT and buoy 41001 whenever the following criteria were met:

- 1) wind direction at 41001 between 20° and 170° inclusive,
- 2) wind direction at HAT between 310° and 50° inclusive (including calm winds),
- 3) HAT wind directed at least 30° but no more than 120° counterclockwise of the wind at 41001,
- 4) wind speed at 41001 of at least 4.1 m s^{-1} (8 kt), and
- 5) air temperature at 41001 at least 3°C greater than the air temperature at HAT.

A similar set of criteria was used to identify fronts between ILM and buoy 41002. Once all the criteria were met for six consecutive hours, the onset of the front was defined as the first hour when all criteria were found.

In the second stage of the identification process, hourly frontogenesis was computed from the surface data. The simple method of Sanders (1955) was used wherein diabatic, tilting, and shearing terms are omitted and frontogenesis, F , is computed from

$$F = (\Delta v / \Delta y)(\Delta T / \Delta y), \quad (1)$$

where the y axis is oriented perpendicular to the surface front and directed toward the cold air. For lack of precise information, the front is assumed oriented at a constant 40° from north for all cases, as given by the average Gulf Stream alignment. The hourly temperature, wind speed, and wind direction at the land–buoy pairs were used in the calculation. A horizontal distance, Δy , of 309 km was used for the northern and 320 km for the southern pair.

Manual validation of the identification method was accomplished by comparison with National Meteorological Center [NMC, now known as the National Centers for Environmental Prediction (NCEP)] 3-hourly surface analysis charts. All coastal fronts were identified from the NMC charts for an 11-month test period during the winters of 1989–91. In performing this identification, emphasis was placed on the plotted station data rather than the analysis of features. To meet coastal front criteria, surface temperatures and winds reported at coastal and offshore platforms had to re-

semble the pattern illustrated in Fig. 2 for at least two successive 3-hourly maps. The resulting list of cases was cross checked with cases identified by our four-station algorithm.

Results of the cross check showed excellent agreement between the NMC analyses and the objective algorithm. For 20 out of 34 test cases, the two methods agreed. For those remaining, there was an even split with seven cases evident on the maps but missed by the algorithm, and seven detected by our algorithm but not evident on the surface maps. All but 2 of these 14 cases either dissipated soon after forming or moved ashore quickly and hence did not meet our 6-h persistence criterion. Since the NMC charts are available only at 3-h intervals, some overcounting was not unexpected. Although no such cases were found in the sample, there is some possibility that a few synoptic-scale warm fronts or land-breeze systems are included by our algorithm. However, composite maps (to be discussed later) suggest that the inclusion of warm fronts is rare.

A coastal front was considered a single case for as long as the preceding criteria were met. If there was a gap of 6 h or less during which one or more of the criteria were not met, then the event was considered a single case. Otherwise the event was considered two separate cases. The interval of 6 h was chosen based on review of coastal front cases from the NMC analysis maps and the minimum time needed for the overall synoptic conditions to change significantly. The above algorithm was applied to hourly data from 1984 through 1994—a convenient 11-yr sample of sufficient length and data coverage to yield a large sample of coastal fronts.

Once the front was detected offshore, a method was developed to detect its onshore movement. Three stations were used, namely Raleigh–Durham (RDU), HAT, and ILM. It was determined that for a coastal front to be classified as making landfall at either HAT or ILM, all the following criteria must have been met:

- 1) a clockwise wind shift of at least 20° at HAT/ILM over a 1-h period (i.e., between two consecutive observations),
- 2) an increase in air temperature and dewpoint of at least 2°C at HAT/ILM over a 2-h period (with the increase observed within an hour of wind shift),
- 3) wind direction at HAT/ILM of between 30° and 180° inclusive after the wind shift, and
- 4) air temperature at HAT/ILM of at least 2°C greater than the air temperature at Raleigh at the hour after the temperature increase.

The modest temperature change in criteria 2 and 4 is to ensure that even weak fronts are included in the

initial sample. The specified increase in dewpoint is set to signal the arrival of a postfrontal marine air mass. Together with the other criteria, there were no misses or false alarms based on checks against NMC map analyses.

The above criteria were applied to all offshore fronts identified from the 11-yr sample. The cases were then sorted into categories based largely on their onshore movement. For each category, NCEP–National Center for Atmospheric Research (NCAR) reanalysis data (Kalnay et al. 1996) were used to compute composite fields for several standard variables such as sea level pressure, temperature, relative humidity, wind speed, and geopotential height.

3. Results and discussion

a. Seasonal and CAD-related averages

A total of 379 coastal fronts were identified for the 11-yr period. The cases were sorted into three broad categories, namely: offshore fronts, onshore fronts, and diurnal fronts. The offshore category consisted of fronts that did not pass either ILM or HAT. These comprised 112 cases or 30% of the total. Onshore fronts, defined as fronts that formed offshore and subsequently passed either ILM or HAT, were less frequent with 70 cases or 18% of the total. Note that because the algorithm requires that warming be associated with frontal passage, sea-breeze fronts are not included in this category. Finally the diurnal subtype included offshore fronts that did not appear to be present at 1800 UTC. This diurnal subtype resembles the type B front found by Nielsen (1989) in his climatology of New England coastal fronts. In our case, the diurnal fronts generally formed at night and disappeared by late morning, with about half the cases appearing on several successive nights. Typically, these types occurred during onshore geostrophic flow, as will be described in more detail later. It is presumed that many of these phenomena were associated with the nightly contrast between the stable planetary boundary layer over land and the neutral marine boundary layer and therefore may represent fronts that are especially shallow. Thus, the cases in this diurnal category likely range upward in scale from land-breeze fronts to classical offshore fronts. Even though they seem to be based on surface features and lack temporal persistence, diurnal fronts should be considered true mesoscale frontal systems. For example, Sanders and Doswell (1995) argue that local surface-based zones of thermal contrast constitute true mesoscale fronts and these authors deemphasize the importance of extended temporal persistence. In our case, the

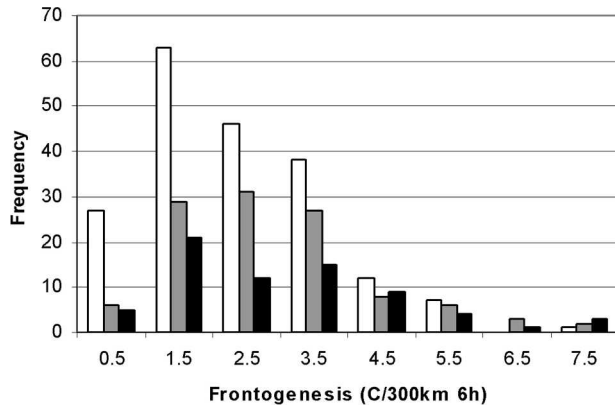


FIG. 3. Frequency distribution of frontogenesis for diurnal (clear), offshore (shaded), and onshore (black) coastal fronts for all seasons for 1984–94. Frontogenesis values represent averages computed for the first 6 h after detection.

diurnal category represents 197 cases or just over half the total.

The average frontogenesis for the first 6 h after detection was $2.60^{\circ}\text{C} (300 \text{ km } 6 \text{ h})^{-1}$ ranging from 2.33° for diurnal to $2.93^{\circ}\text{C} (300 \text{ km } 6 \text{ h})^{-1}$ for onshore classifications. The distribution of this measure is illustrated in Fig. 3, and as expected, it is skewed toward stronger frontogenesis cases that occur less frequently. Despite their large numbers, diurnal types are not well represented among strong fronts. One may argue that the small number of strong diurnal fronts is expected since weaker fronts are more apt to dissipate during the daylight hours and diurnal fronts are defined by this very characteristic.

Earlier case studies by Riordan (1990), Nielsen (1989), and Bosart et al. (1972) demonstrate that the horizontal spatial scale for coastal fronts is of the order of 100 km and typical frontogenesis values are roughly 5–10 times those given here. This contrast is consistent with our coarse Δy of 300 km imposed by the station spacing and suggests that values given here are best used for relative comparison among cases rather than for comparison with other types of fronts.

While data were rarely missing from both buoys (only 4% of the time), there was a significant number of days (43%) when all data from one buoy were absent. Data coverage at the buoys was generally more complete in late summer and fall and less so in winter and early spring. Because the missing data were not evenly distributed throughout the year, one cannot use our sample for much discussion of the seasonality of coastal fronts. However, one can still make several clear inferences. For example, as was found elsewhere by Bosart (1975), coastal fronts were more frequent in winter than in summer. Specifically there were a total of 253

cold-season events (defined as 16 October–15 April) even though these were less likely to be detected because of missing buoy data. Many fewer cases (126) were detected in the warm season (16 April–15 October). Furthermore, onshore and offshore categories together represented 61% of the cold-season cases, but only 21% of the warm-season events, leaving the diurnal cases to dominate the warm season.

Excluding the diurnal cases, 80 of the cold-season coastal fronts were associated with regional CAD as determined by Bailey et al. (2003) for the same dataset (Table 1). These cases represent only 52% of all cold-season onshore and offshore coastal fronts. Bailey et al. defined CAD by the Laplacian of the sea level pressure and surface potential temperature computed from a nine-station grid. The grid was centered over the Piedmont of the Carolinas and Virginia and extended from the coast northwest to the Appalachians. While the weak association may seem surprising, coastal fronts can develop in response to more localized processes such as direct thermal circulations at the Gulf Stream edge or ahead of northward-moving coastal cyclones not associated with CAD. Furthermore, a broad surface pressure ridge centered east of the Piedmont might not qualify as a CAD event, but it could support an offshore coastal front with its inverted trough well offshore. The fact that more than twice as many non-CAD coastal fronts are offshore types as opposed to onshore seems to agree with this notion.

Nearly all of the onshore fronts (97%) occurred in the cold season and most (63%) were accompanied by CAD. At the other extreme, half of the diurnal fronts occurred in this season, but only 15% of these coincided with a CAD event. As will be discussed later, the possible explanation for this contrast may lie in the differences in dynamics associated with diurnal fronts.

In the warm season when onshore fronts are ex-

TABLE 1. Distribution of coastal front (CF) types with cold-air damming (CAD) and with season for the period 1984–94. Cold-season cases include those that begin in the period 16 Oct–15 April and warm-season cases include those that begin in the period 16 Apr–15 Oct.

CF Type	With CAD	Without CAD	Total
Onshore			
Cold season	43	25	68
Warm season	0	2	2
Offshore			
Cold season	37	50	87
Warm season	12	13	25
Diurnal			
Cold season	15	83	98
Warm season	26	73	99

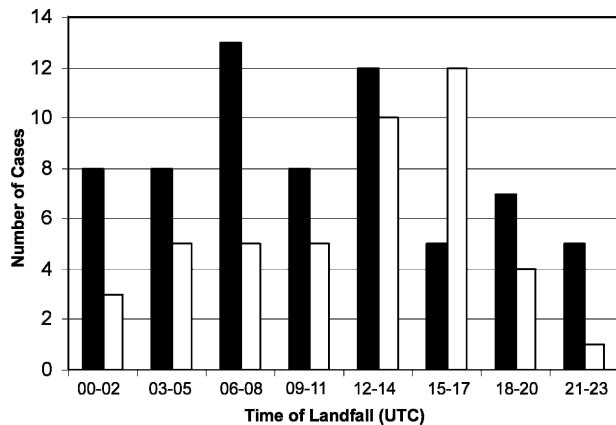


FIG. 4. Times of coastal front passage at Wilmington (clear) and Cape Hatteras, NC (black).

tremely rare, the offshore types occur at about equal frequency with or without CAD. In this season, diurnal fronts still generally occur without CAD, although the association seems to be stronger than in the cold season. This observation is a bit puzzling since dynamics and frontal zones are generally weaker in summer and it is, therefore, logical that the link between the two phenomena would be more random.

Onshore fronts passed HAT more often than ILM, a result not surprising when the shape of the coastline is considered. Specifically, 44% made landfall at both HAT and ILM, 41% made landfall at only HAT, and 14% made landfall only at ILM. In this connection, it was not considered necessary for a coastal front to be identified offshore of a particular station for landfall to be detected at that station. For example, when data from the northern buoy were missing, a front could only be detected off ILM. However, if the signature of frontal passage were later detected at HAT, it was attributed to coastal front passage.

Just as there was an annual cold-season preference for onshore frontal movement, there was in some cases a diurnal preference. At ILM, fronts were most likely to move onshore during the early daylight hours (Fig. 4). However, at HAT the pattern is somewhat different as an indistinct maximum occurred sometime between 0600 and 1400 UTC and few fronts passed during the subsequent daytime hours. It may be that HAT is more characteristic of an ocean station since it is located on Hatteras Island roughly 50 km east of the mainland, while the reporting site at ILM is located 13 km inland from the coast. Here, absorption of solar energy by the land surface in the morning may warm the shallow cold air and allow the front to move inland readily. Such behavior was observed in an earlier case study (Riordan 1990).

b. Temperature and precipitation averages

Coastal fronts are usually accompanied by significant changes in sensible weather and thus are important to forecasters. This section provides quantitative examples of how frontal passage relates to local changes in temperature, wind direction, and precipitation. Figure 5 shows the average hourly trends in temperature centered at the time of landfall for HAT and ILM (negative numbers denote hours before landfall). For this comparison, hourly temperature changes were computed relative to the value 6 h prior to frontal passage and results were averaged for all onshore fronts. At both sites there is a large jump of about 3°–4°C in the hour prior to the wind shift—a pattern that resembles a classical warm front. After frontal passage, there is continued warming at ILM, but this trend is not evident at HAT.

Wind shifts associated with frontal passage are comparable at both sites but at ILM (Fig. 5d) the wind speeds increase more markedly after frontal passage. Both this tendency and the postfrontal warming at ILM may be related to the tendency for frontal passage at that site during the morning. Thus, both tendencies may simply be attributed to normal diurnal variations.

The number of landfalling coastal fronts that brought measurable precipitation within 6 h of landfall was much larger for ILM than for HAT. For example, of the 60 coastal fronts identified as making landfall at HAT, only 18% had precipitation within 13 h centered at frontal passage, while at ILM, 86% of onshore fronts produced precipitation. The reason for this marked contrast may be related to differences in static stability or to the fact (demonstrated in section 3d) that ILM generally lies closer to an approaching cyclone and therefore may typically be in a zone of stronger thermal contrast.

For cases where precipitation occurred anytime within 6 h of landfall at ILM, precipitation was most frequent in the hours preceding frontal passage (Fig. 6). Approaching the hour of frontal passage, the number of fronts with precipitation increases steadily but is followed by a dramatic decrease. Total rainfall for onshore frontal events is sometimes appreciable (Fig. 7) as most cases had precipitation greater than 2.5 mm and 10% had over 25 mm.

Extending the discussion of frontal passage to all regional coastal and offshore sites with sufficient data records, one sees interesting patterns. Figure 8a presents the average change in wind direction accompanying frontal passage. The sites are listed in the legend in order of their average distance from the Gulf Stream. For example, Diamond Shoals (DS) is closest to the

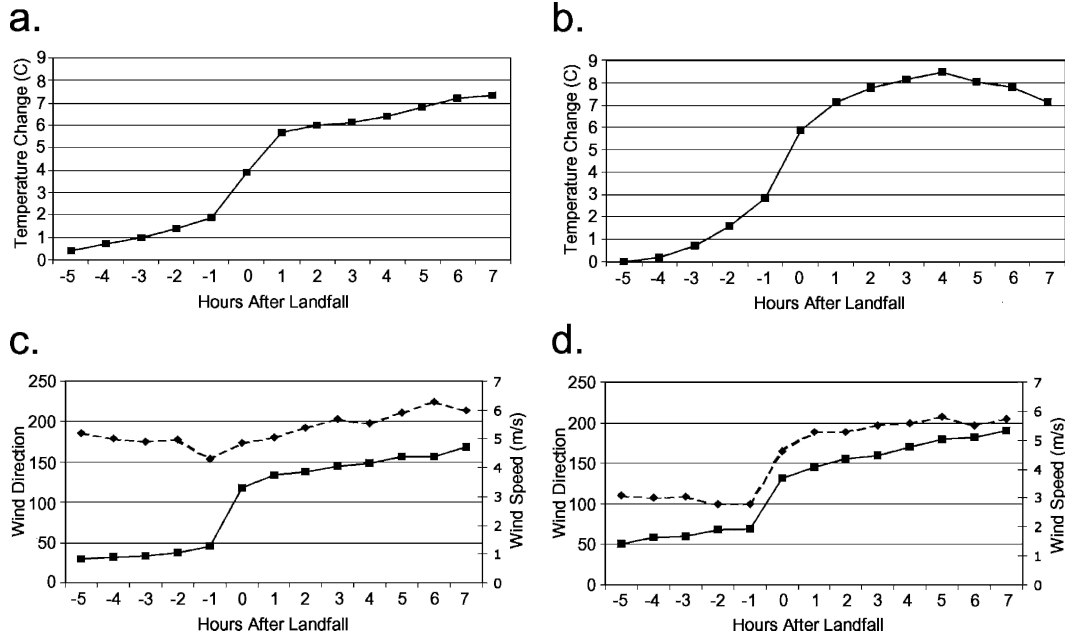


FIG. 5. Average changes in temperature and winds accompanying coastal front passage: temperature change starting 6 h before frontal passage at (a) Cape Hatteras and (b) Wilmington; wind direction (solid) and wind speed (dashed) at (c) Cape Hatteras and (d) Wilmington.

edge of the warm water and Cape Henry Light Tower (CHL) is farthest. It can readily be seen that at the hour of frontal passage, the wind shift can average as much as 60°–80°. Moreover, the magnitude of the wind shift generally diminishes with increasing distance from the Gulf Stream.

A similar signature is observed in the temperature records, summarized in Fig. 8b. A typical warming of up to 3°–4°C occurs at frontal passage and its magnitude generally decreases systematically with distance from the Gulf Stream. However, there are two important exceptions, namely, CHS and ILM, the only two inland sites. Here the warming is much more pro-

nounced and extends more noticeably into the post-frontal hours. It should be noted that only at these two sites is the frontal passage most frequent during the morning. Thus, some of the observed warming can be attributed to the diurnal cycle.

Although sea surface temperature (SST) records are not available from all sites, it seems likely that the association of frontal strength with Gulf Stream distance may be related to the general observation that in winter, the sea temperature decreases shoreward of the Gulf Stream. At Duck Pier (DUK) and CHL the SST is generally the coldest of all sites, and here the average

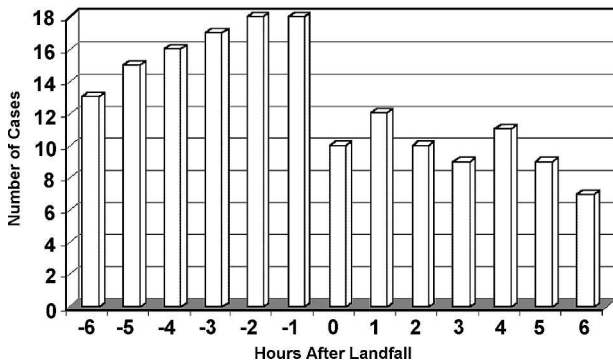


FIG. 6. Number of coastal front cases with measurable precipitation at Wilmington, shown hourly and centered at the time of frontal passage.

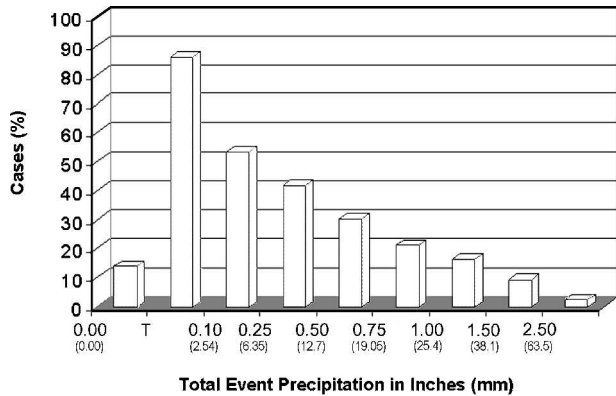


FIG. 7. Percent of cases exceeding threshold precipitation at Wilmington for the period from 6 h before to 6 h after frontal passage.

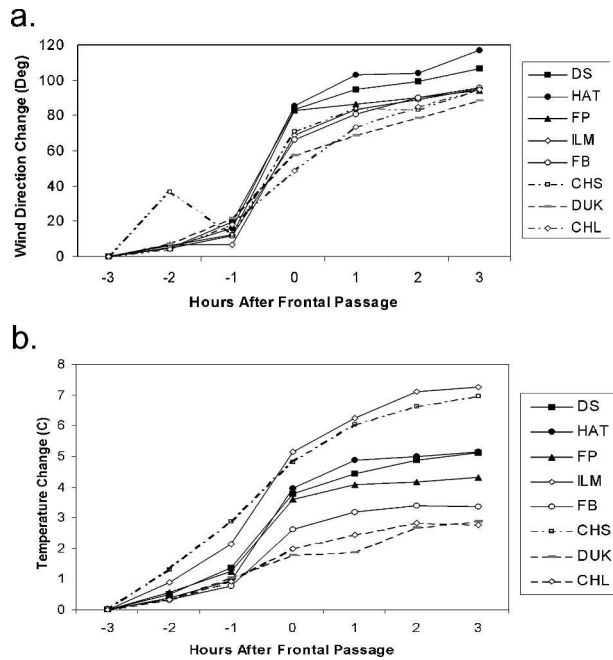


FIG. 8. Average change in (a) wind direction and (b) temperature starting 3 h prior to frontal passage at selected sites. See Fig. 1 for site locations.

frontal passage is barely detectable in the temperature record.

A recent example from 5 December 2003 is illustrative of the ambiguous nature of the frontal passage at the northern sites in the study area. For this case, time series for temperature and wind direction show classic frontal passage at Cape Hatteras (now designated HSE), but are difficult to interpret at Cape Henry Light Tower (now CHLV2) and a new buoy to the east-southeast (44014). Figure 9 shows the dramatic thermal SST contrast in the region for this case. The Gulf Stream veers offshore near Cape Hatteras and much colder waters lie to the northwest, as is typical of winter. Thus, both CHLV2 and 44014 lie in the cold waters, with the buoy reporting an SST value of 13.4°C.

Figure 10 presents a sequence of surface analyses starting at 0000 UTC when the front lies just off Cape Hatteras and has a structure of a classic warm front. As time progresses, the thermal gradient continuously builds in the warm air such that by 0900 UTC (Fig. 10d) the wind shift and pressure trough lie within the gradient. In fact, over the colder waters north of the Gulf Stream the exact location of the surface front is ambiguous.

c. Case composites

Since forecasting the inland movement of coastal fronts represents an important problem, we might ask if

there is synoptic-scale evidence that can be used to help differentiate, a priori, the fronts that stay offshore from those that move inland. If such were the case, forecasters might be provided with signals in, for example, the sea level pressure or 500-hPa height field that would relate to later frontal behavior, and if such were the case, composites of synoptic-scale conditions prior to onshore movement might also provide evidence of physical processes consistent with onshore frontogenesis.

Determining the composite-mean and variance of surface and upper-air map fields for each frontal category would seem especially useful in this endeavor and the NCEP–NCAR reanalysis data are well suited to this purpose. For example, Lackmann et al. (1996) used composites of NCEP–NCAR reanalysis data to describe the distinguishing features of explosive cyclogenesis in the North Atlantic. Bailey et al. (2003) identified synoptic patterns associated with regional CAD, and Bell and Bosart (1989) established the utility of compositing for identifying distinguishing large-scale features attending New England coastal fronts.

One limitation of the NCEP–NCAR reanalysis data for our present study is their coarse (2.5° latitude by 2.5° longitude) spatial resolution and 6-h temporal resolution. Coastal fronts are mesoscale features and will not be well resolved. However, attendant synoptic features are of primary interest here and will be emphasized.

In selecting cases for compositing, several additional criteria were added to the basic identification algorithms. First, to ensure that marginal cases were eliminated, only cold-season fronts where the average F was greater than $1.00^{\circ}\text{C} (300 \text{ km h})^{-1}$ were included. As was done previously, F was computed over the first 6 h after frontogenesis. Second, to eliminate sampling bias, cases were included only if data from both buoys were present.

An effort was also made to ensure that weak onshore fronts were eliminated. Starting at times when offshore frontogenesis was noted, hourly records from four nearshore sites were inspected for temperature and wind signatures characteristic of warm-frontal passage. These four sites included C-MAN stations at Diamond Shoals and Frying Pan Shoals as well as the original coastal sites at HAT and ILM. For cases included in the compositing sample, it was found that the average wind direction prior to frontal passage was 40° followed in 3 h by a clockwise shift of 80° and a mean temperature increase of over 4°C . In almost every case, the warming proceeded at an increasing rate until an abrupt wind shift occurred. The limits for admissible

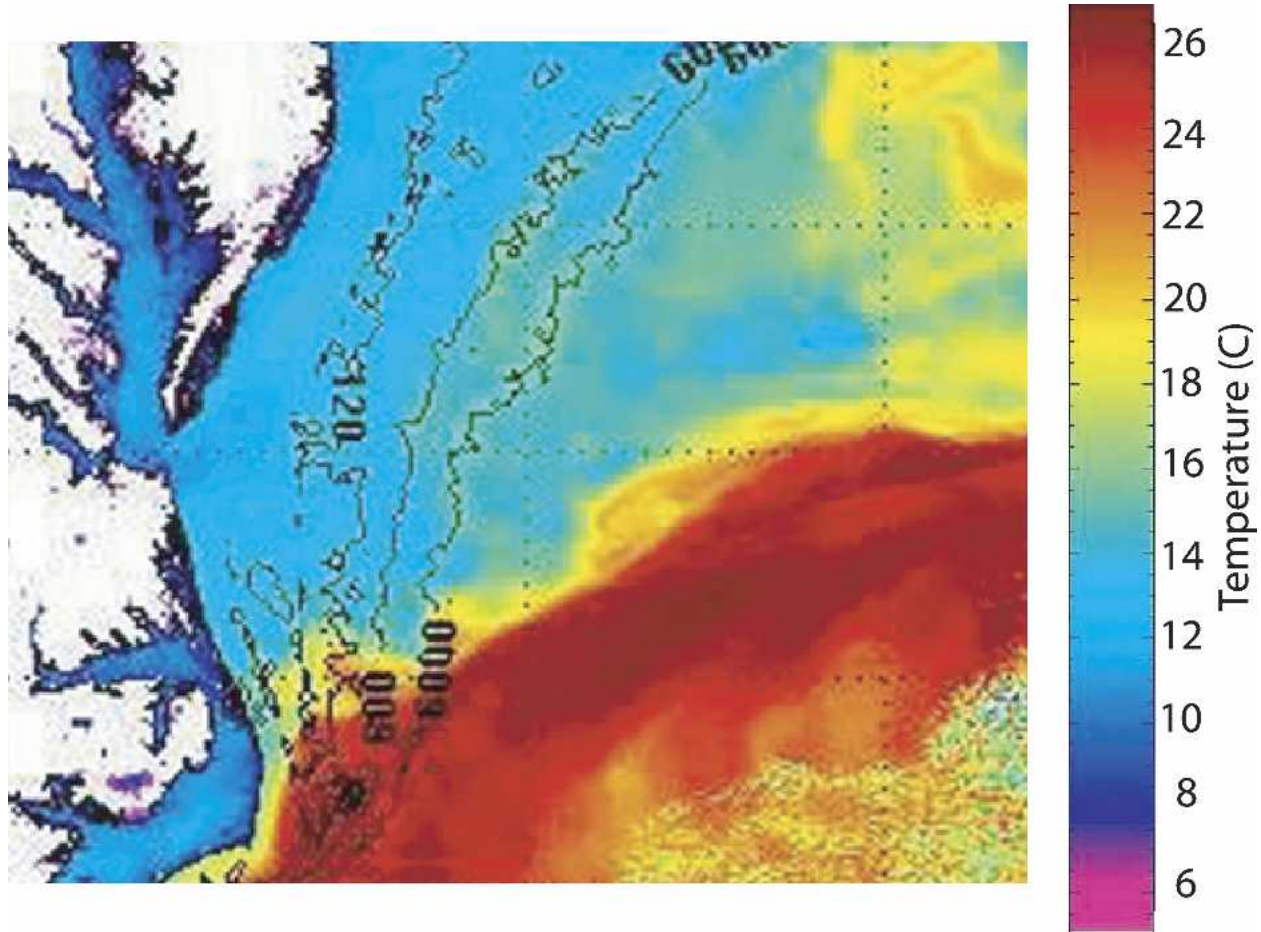


FIG. 9. Infrared image of SST as measured from *NOAA-I6* at 0749 UTC 1 Dec 2003. (Courtesy Rutgers Marine Data; available online at http://marine.rutgers.edu/mrs/sat_data/?product=sst¬humbs=1.)

3-h temperature change, ΔT , and wind direction change, ΔWD , for the sample are

$$1.8^{\circ} < \Delta T < 10.0^{\circ}\text{C} \quad \text{and} \quad 30^{\circ} < \Delta WD < 160^{\circ}.$$

The initial wind directions for all cases lay between 340° and 80° . Often frontal passages that appeared weak at one site displayed strong signatures at another. For example, the frontal passage at Frying Pan Shoals at 0700 UTC on 2 March 1994 was accompanied by a warming of only 1.8°C , and a wind shift from 80° to 120° . However, a few hours later, a warming of 6.9°C and a shift from 50° to 140° occurred at nearby ILM.

Finally, to increase the likelihood that the cases used to build the composites represent independent events, cases were excluded if they began within 96 h of the termination of a preceding case. This threshold seems reasonable in light of findings by Chiu (1973), Hartmann (1974), and Barber et al. (1984) who found a synoptic-scale period of 2–5 days in the midlatitudes in winter.

After the selection process, in the 11 cold seasons there remained 33 cases of offshore fronts, 35 onshore fronts, and 41 diurnal fronts. All the composites were centered at the 6-h time (0000, 0600, 1200, or 1800 UTC) closest to the onset of offshore frontogenesis. A two-sided Students' *t* test was used to evaluate the statistical significance of features in the composites. The test assumes a normal distribution of data. Figure 11 shows the frequency distribution of mean sea level pressure (MSLP) for one grid point taken from the reanalysis grid sets. The grid point is located in the northeast United States where one would expect a large range of pressures over the course of a typical year. Although it is hard to argue that any particular point represents the whole, given the well-behaved distribution of MSLP in Fig. 11, it appears that one can be reasonably confident in using the Students' *t* test as a measure of statistical significance. Our null hypothesis states that there is no significant difference among frontal types. Computed sig-

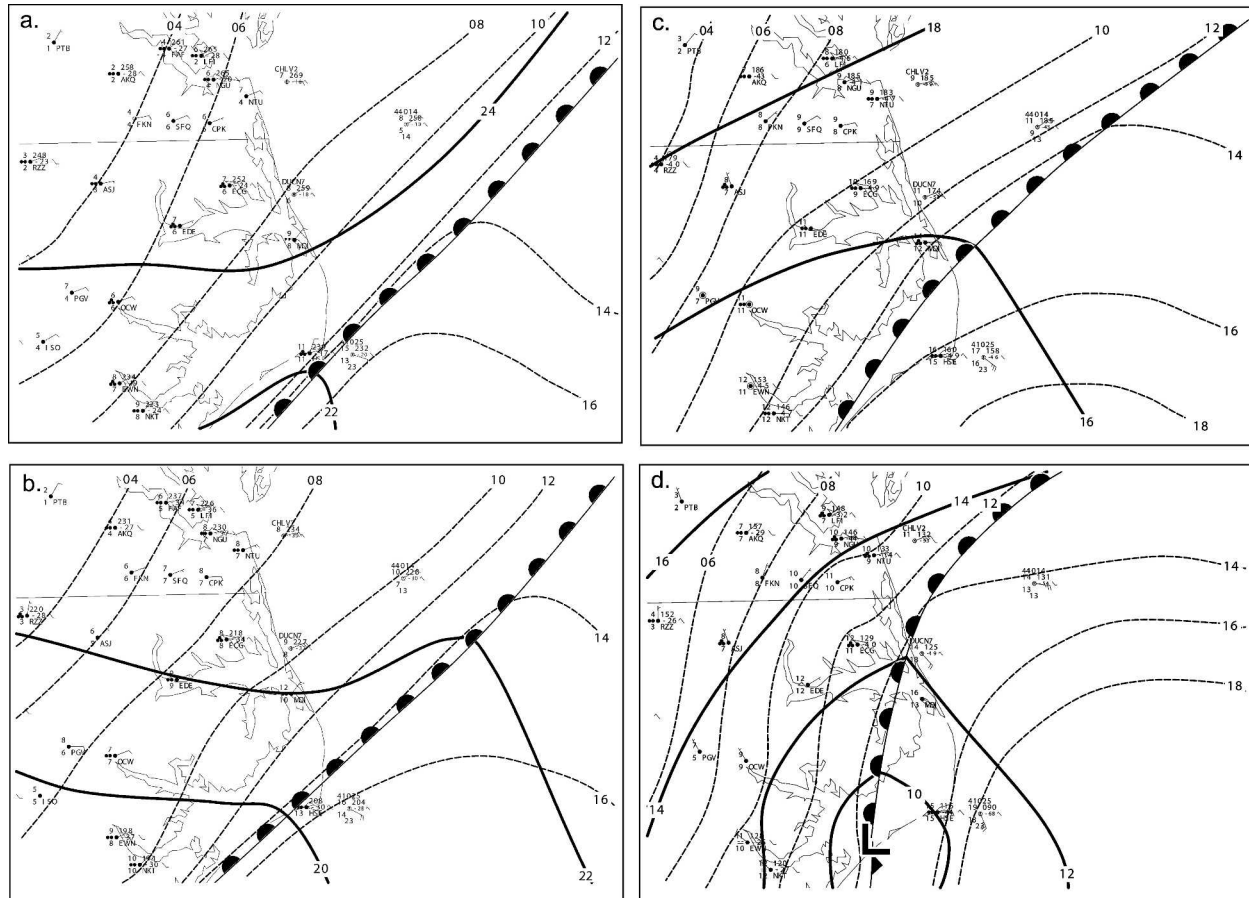


FIG. 10. Surface analyses of sea level pressure (solid lines labeled in hPa) and temperature (dashed lines labeled in °C) for 5 Dec 2003 at (a) 0000, (b) 0300, (c) 0600, (d) 0900, (e) 1100, and (f) 1200 UTC.

nificance values indicate confidence in rejecting this hypothesis.

d. Composite intercomparison

Composite maps serve to illustrate general similarities among onshore, offshore, and diurnal coastal fronts. For all three types, the sea level pressure field is dominated by a synoptic-scale anticyclone centered north of the Carolinas (Fig. 12). In all three cases the anticyclone center moves eastward from a location near the Ohio Valley some 12–24 h prior to coastal frontogenesis. By the time of initial offshore frontogenesis, an inverted ridge extends from the parent high across the Piedmont region east of the Appalachians suggesting that CAD is in progress. It is interesting to note that even though the NCEP–NCAR reanalysis data are spatially coarse, there is clear evidence in all three composites of an inverted trough offshore resembling a coastal front starting at the time of frontogenesis. The enhanced thermal gradient west of the trough is also suggestive of coastal front structure.

However, there are important large-scale differences that distinguish each individual coastal front category from the other two. The onshore frontal type is characterized by progressive eastward motion of the parent anticyclone. At 12 h prior to frontogenesis, a cold front has exited the East Coast as seen by the pressure trough and accompanying band of high relative humidity in the western Atlantic in Fig. 12a. In the next 24 h the front continues to sweep eastward as the anticyclone moves offshore and establishes a wide zone of warm advection across the Southeast as cyclogenesis begins in the Gulf of Mexico (Figs. 12b,c). Note that the eastward progression of the anticyclone seems to preclude the arrival of synoptic-scale warm fronts from the east.

The onshore composite also is unique in that it suggests cyclogenesis in the Gulf of Mexico at about the time of coastal frontogenesis. Inspection of NCEP–NCAR fields for individual onshore cases nearest the time of frontogenesis showed that a surface trough or closed low was present in the central or western Gulf of Mexico 74% of the time.

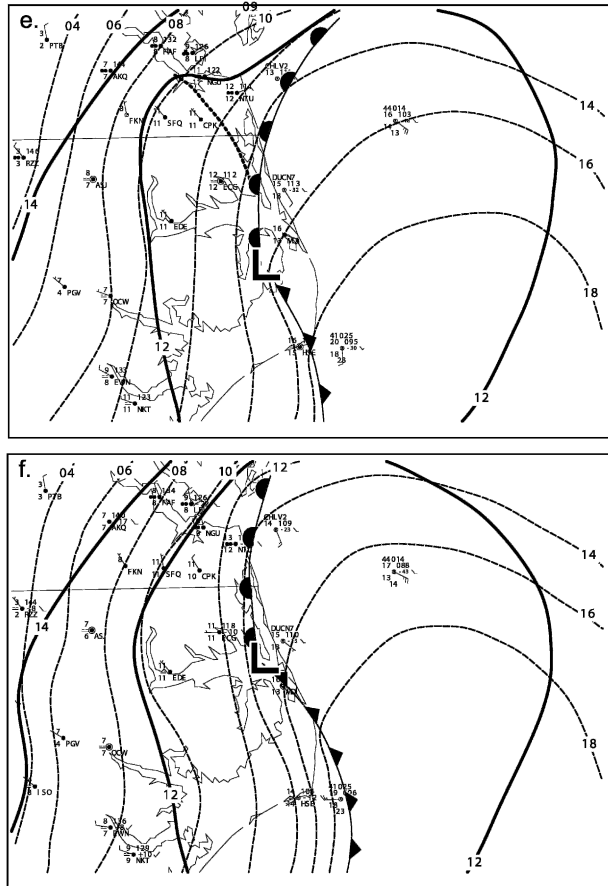


FIG. 10. (Continued)

At the time of frontogenesis and thereafter, onshore geostrophic flow at the surface and implied isentropic ascent associated with warm advection are consistent with high relative humidity across the Southeast also seen in the composites. These features are also supportive of developing warm frontal conditions aloft across the Carolinas. Furthermore, studies by Nielsen and Neilley (1990) and Riordan et al. (1995) have demonstrated that landward movement of the offshore coastal fronts is consistent with density current theory. In this framework, a major flow component toward the west and northwest on both sides of the front, as is suggested here by the onshore geostrophic flow near the surface, facilitates landward motion of the front.

The onshore composites share much similarity with synoptic conditions associated with New England coastal frontogenesis as reported by Bell and Bosart (1989). In their study, composites of the large-scale flow were constructed for 11 cases of coastal frontogenesis. The relative location and intensity of the surface cyclone, anticyclone, and the 500-hPa trough at the time of frontogenesis off New England shown in their com-

posites are strikingly similar to ours. The orientation of the axis of the anticyclone as it nears the coast is even nearly identical in both cases. Evidently, New England coastal frontogenesis occurs under the same type of synoptic conditions favoring fronts that move ashore in the Carolinas.

Several important features differentiate the offshore composite from the onshore type. For the offshore composite, the anticyclone stalls at the New England coast and there is seldom Gulf cyclogenesis. Specifically, at the time of frontogenesis, a closed surface low was evident in the central and western Gulf only 10% of the time. If weak troughs are included, the percentage increases to only 30%.

Also seen in the offshore composite is negligible warm advection along the Southeast coast as ridging persists inland. In contrast with the onshore type, there is little onshore flow in the Carolinas and the air inland remains drier at low levels (Figs. 12d–f). Furthermore, these differences become more pronounced with time starting at frontogenesis. However, even though the onshore and offshore composites are dynamically consistent, the coastal isobar orientation is not in itself a clear indication of onshore versus offshore type. Figure 13 illustrates the orientation of the surface geostrophic wind vector at the onset of each onshore and offshore case. The orientation was determined from the NCEP–NCAR sea level pressure field and was measured at the coastline at the North Carolina–South Carolina border. The 500-km section of coastline centered here is oriented at about 240° . Thus, a reasonable offset of 20° between the isobar orientation and surface winds places the modal surface winds for offshore cases at almost exactly parallel to the coast. By contrast, the distribution for the onshore cases is shifted roughly 30° clockwise and, therefore, is directed more inland. However, there is considerable scatter for onshore cases and a large number are practically coast parallel also. Reliance on isobar orientation alone would yield mixed results.

Persistent surface ridging across the south is even more pronounced for the diurnal type (Figs. 12g–i). In this composite, the parent high becomes increasingly elongated in the east–west direction as its center progresses offshore. The pressure gradient and the relative position of the anticyclone in this composite resemble those accompanying the diurnal type fronts in New England except that for the latter case, the anticyclone is centered farther north (Nielsen 1989). In our case, the surface pressure and thermal gradients are weaker than for the other two cases and warm advection is consequently limited across the Carolinas. Again, Gulf cyclone development is not evident. Seasonality likely in-

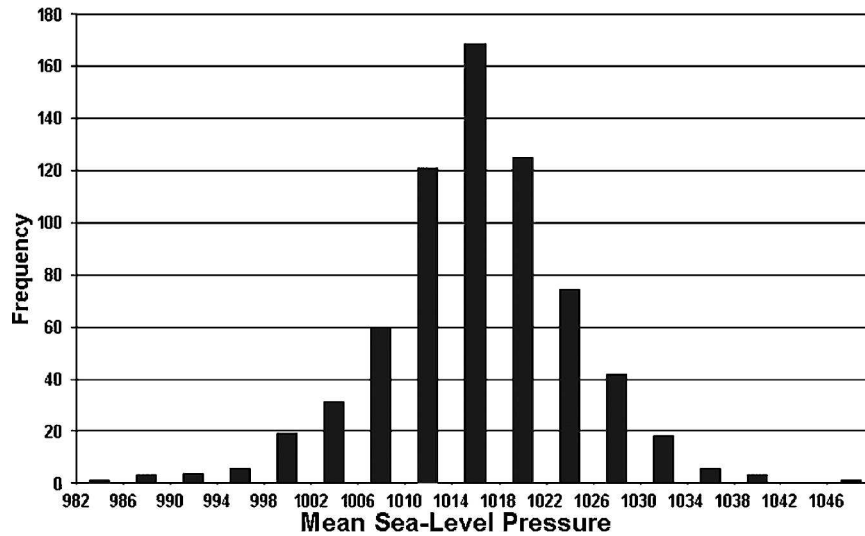


FIG. 11. Frequency distribution of mean sea level pressure (hPa) from the NCEP-NCAR reanalysis dataset. Pressures were sampled every 10 days at 0000 UTC for 20 yr for the grid point located over south-central New York (grid point 115, 18 in the reanalysis dataset).

fluences this composite because two-thirds of the diurnal cases occur outside the core winter (December–February) period when less than half the onshore and offshore types occur. Thus, it is not entirely surprising that gradients are weaker for the diurnal type.

The persistent environment of the broad zone of weak onshore geostrophic flow for the diurnal type is consistent with the observed unique tendency for diurnal coastal fronts to redevelop on successive nights. For this type, drier conditions prevail inland as evidenced by low relative humidity and ridging across the Southeast. Thus, one may assume that limited cloudiness and therefore enhanced solar insolation during the day probably reduce the thermal contrast between buoys 41001 and 41002 and the coastal sites at ILM and HAT. This differential heating would account for the apparent demise of the diurnal coastal front each morning. It is possible, however, that the diurnal front may persist offshore during the day in the zone between the Gulf Stream and the colder shelf waters.

The development of the Gulf low and the progression and shape of the parent anticyclone are surface features that, taken together, distinguish the three types. Figure 14a illustrates the difference fields generated by subtracting the sea level pressure fields for the offshore from the onshore composite. By the time of frontogenesis, there is an area of negative pressure difference extending from the western Gulf of Mexico northward across the Mississippi and Ohio Valleys. From the Student's *t* test, one can be 99% confident that this difference is significant. Thus, the presence of the Gulf low and inverted trough extending north to-

ward the Great Lakes in the onshore composite probably does not result from a few individual cases, but characterizes the type. In general, significant differences increase with time and move eastward in the wake of the parent anticyclone (not shown).

The significant Gulf low also appears in the onshore–diurnal difference field (Fig. 14b). For this composite there is also an area of positive difference near the Great Lakes. Comparison with Figs. 12g–i shows that this difference is due to the surface low approaching the lakes, but perhaps more importantly, the associated retreat of the anticyclone toward the southeast.

Figure 15 further illustrates the difference in onshore low-level flow and warm advection for the three composites. It is apparent that for the onshore type at 925 hPa, onshore geostrophic flow, warm advection, and probably moisture transport dominate the Southeast. For the offshore type, there is also onshore flow and warm advection especially from South Carolina southward, but the geostrophic warm advection along the Carolina coast is approximately half that of the onshore case. For the diurnal type, there is negligible warm advection along the Southeast coast.

So far we have seen that the many features at low levels in the composites appear to be appropriately consistent with expected frontal behavior. Consistency also appears to be true for upper-level features. For example, Fig. 16 shows a progressive weakening in dynamics from onshore to diurnal types. In Figs. 16a–c a relatively sharp 500-hPa trough progresses eastward across the Great Plains to just west of the Mississippi

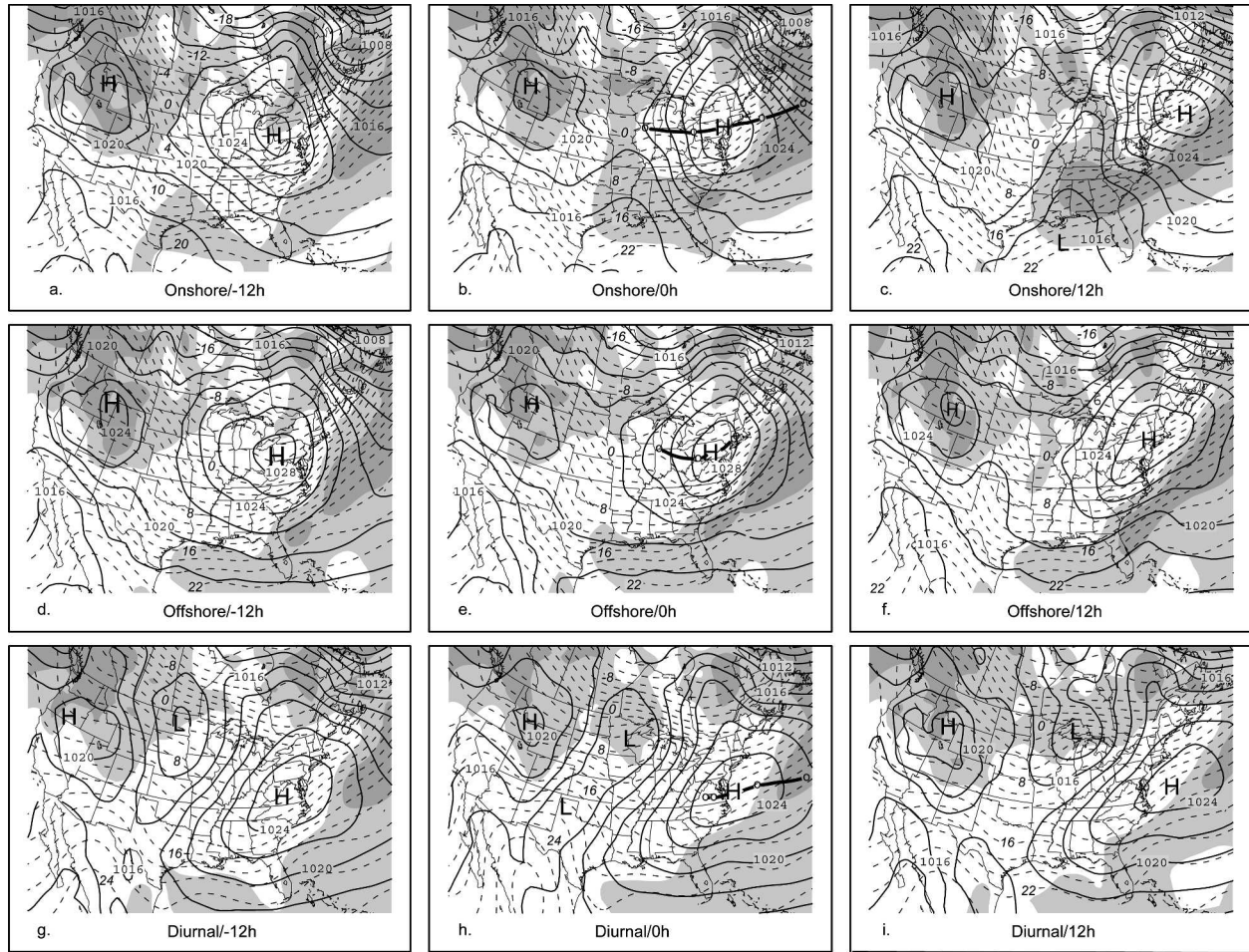


FIG. 12. Composite means of sea level pressure (solid lines labeled in hPa), 1000-hPa temperature (dashed lines labeled in $^{\circ}\text{C}$), and 925-hPa relative humidity (areas with values of 80% or higher are indicated by light shading while those of 90% or higher are indicated by darker shading). Gray dots indicate 12-hourly positions of the center of the anticyclone. (a)–(c) Composite maps for onshore-type coastal fronts at 12-h intervals centered at the time of offshore frontogenesis (0 h), and composites at 12-h intervals for (d)–(g) offshore and (g)–(i) diurnal types.

Valley by the time of initial frontogenesis for the onshore composite. This location provides synoptic-scale ascent that supports the development of low pressure at the surface in the Gulf and troughing in the Mississippi Valley. Confluence well ahead of the trough is consistent with subsidence and maintenance of the surface anticyclone, but the intensification of the 250-hPa jet core over New England and its associated increased ageostrophic ascent supports falling surface pressure in the Ohio Valley by the time of frontogenesis. The right-entrance region of this jet core moves eastward to near West Virginia 12 h later as the surface anticyclone retreats offshore. For the offshore composite (Figs. 16d–f), trough and jet features and, by inference, ageostrophic effects are weaker. In the diurnal case (Figs. 16g–i) the 500-hPa flow is more nearly zonal and the jet core is located much farther north and away from the

region of interest. The reduction in amplitude of the western trough from onshore to offshore types is significant at the 95% level (Fig. 14c). In the diurnal case, the reduction in trough amplitude is significant at the 99% level. Furthermore, geopotential heights are significantly higher throughout eastern North America for this type (Fig. 14d). Thus, the evidence provided by the composites is both physically and statistically robust.

4. Summary and conclusions

A simple objective method is developed to identify coastal fronts that form offshore of the Carolinas. This method is based on wind and temperature criteria for surface hourly observations at two station pairs that included two sites along the coast (Cape Hatteras and Wilmington, North Carolina) and two moored buoys well offshore.

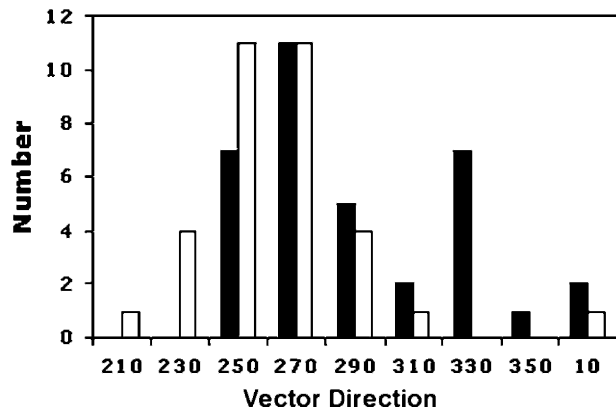


FIG. 13. Direction of the surface geostrophic wind vector ($^{\circ}$) for individual case members of the onshore and offshore frontal composites (black and clear, respectively).

In the 11-yr sample, 379 coastal fronts are identified by this method. Individual cases are sorted into three categories depending on their later evolution. Fronts that persisted through 1800 UTC but never passed either of the two land sites are defined as offshore fronts

and constitute 30% of the cases. Fronts that passed one or both land sites are defined as onshore fronts and make up roughly 20% of the total. Nearly all of these occur in the cold season (16 October–15 April). The remaining cases, constituting most of the total sample, are termed diurnal fronts since they never came ashore and are not detectable at 1800 UTC.

Combined offshore and onshore frontal types constitute about 60% of the cases that occur during the cold season. However, it is surprising that only about half of these combined types are associated with CAD over the Carolinas. If one considers only the onshore fronts, the preference for winter and the link with CAD become much stronger. Nearly all onshore fronts occur in the cold season and over 60% are associated with CAD.

The cold-season preference for frontal activity is as expected, but the result that a large number of fronts (even excluding the diurnal types) appear to be independent of CAD is unexpected. Many forecasters and researchers alike probably link the two phenomena. One reason for their partial independence may be simply due to spatial scale. Conditions conducive to off-

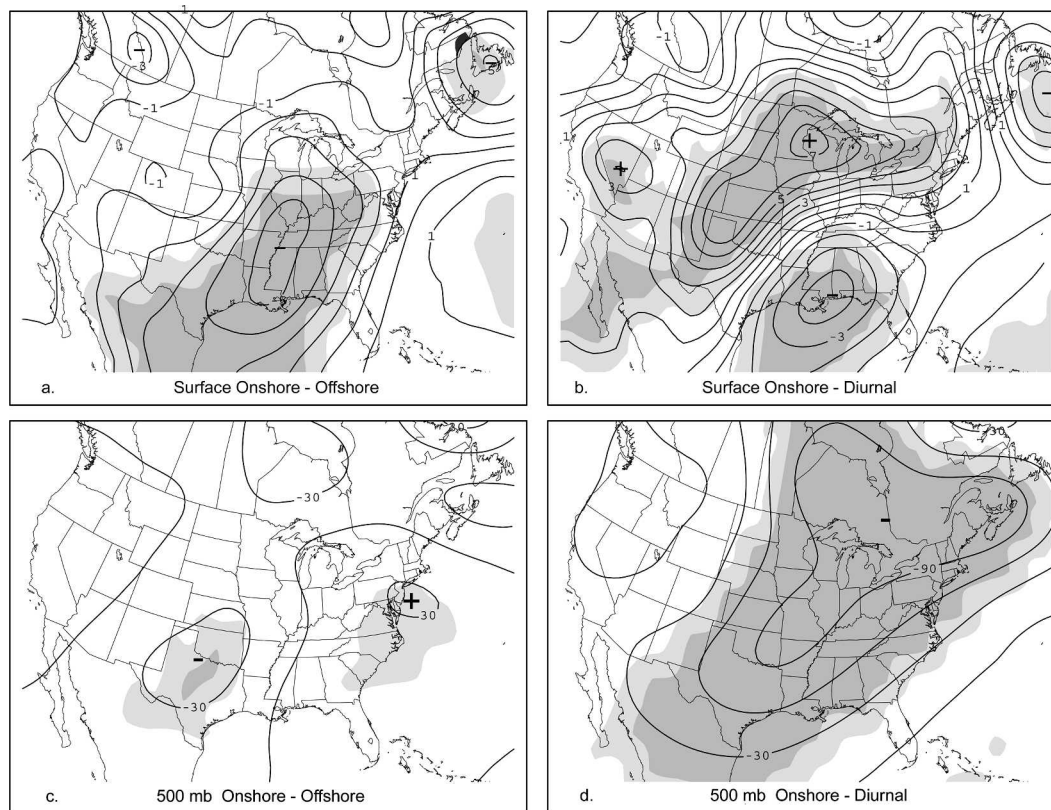


FIG. 14. Difference fields for sea level pressure (hPa) and 500-hPa height (m) for the time of frontogenesis. Contour intervals are 1 hPa and 30 m, respectively. (a), (c) Onshore – offshore composites, and (b), (d) onshore – diurnal composites. Regions where differences are statistically significant at the 95% and 99% levels are indicated by light and dark shading.

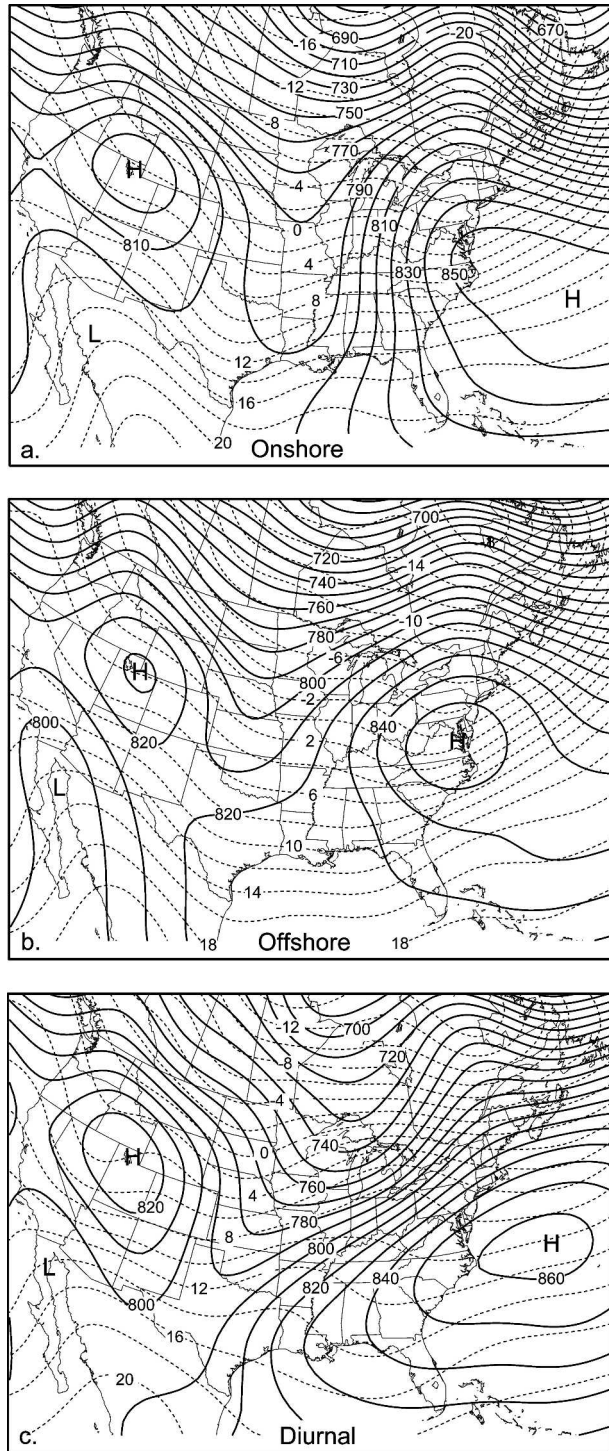


FIG. 15. Composite maps of 925-hPa heights (solid lines labeled in m) and temperatures (dashed lines labeled in $^{\circ}\text{C}$) for the time of frontogenesis for (a) onshore, (b) offshore, and (c) diurnal cases.

shore coastal frontogenesis may occur on a scale much smaller than that of a CAD event. For example, coastal fronts can form north of coastal cyclones even if CAD is absent.

The closer link between onshore fronts and CAD during winter is likely explained by the dynamics. Both onshore fronts and classical CAD are associated with comparatively stronger jet-core dynamics, a deeper 500-hPa trough, and implied evidence of isentropic ascent at low levels. By contrast, diurnal fronts have the weakest association with CAD and have much weaker dynamics. The cold-season preference for onshore fronts and domination of diurnal fronts in summer provides further strong evidence for this dynamic link.

Onshore frontal movement is more common at HAT than at ILM but there is no clear diurnal preference for time of frontal passage. By comparison, at ILM passage is most frequent during early daylight hours, precipitation is much more frequent, and the change in wind speed is greater.

A large wind shift of 60° – 80° and warming of 3° – 4°C during the hour of frontal passage were generally typical of marine and coastal sites closest to the Gulf Stream. Except at the two inland sites (Charleston, South Carolina, and Wilmington, North Carolina), these measures systematically decreased with distance from the warmer waters. Furthermore, at the sites near shore, especially off the southeast Virginia coast, the front was difficult to identify.

At many coastal locations in winter and early spring the shallow shelf waters are much colder than those farther offshore. It is physically consistent that when a coastal front is forced westward over the cold waters, a thermal internal boundary layer (TIBL) likely becomes established in the postfrontal warm air mass. This shallow stable layer is characterized by persistent downward sensible heat flux that would mask frontal passage at the surface and account for the ambiguities seen in frontal analyses. For example, if shear were sufficient, turbulent mixing might scour the TIBL and the front might appear to jump westward. In other cases the front may appear to jump ashore (Riordan 1990).

Composite maps are constructed from NCEP–NCAR reanalysis data for each of the three categories of fronts. Centered at the time of offshore frontal detection, these maps show the average position and strength of synoptic-scale features associated with each category. Principal results of intercomparisons reveal the following:

- A large parent surface anticyclone moving eastward and centered north of the Carolinas is common to all three categories of coastal fronts.

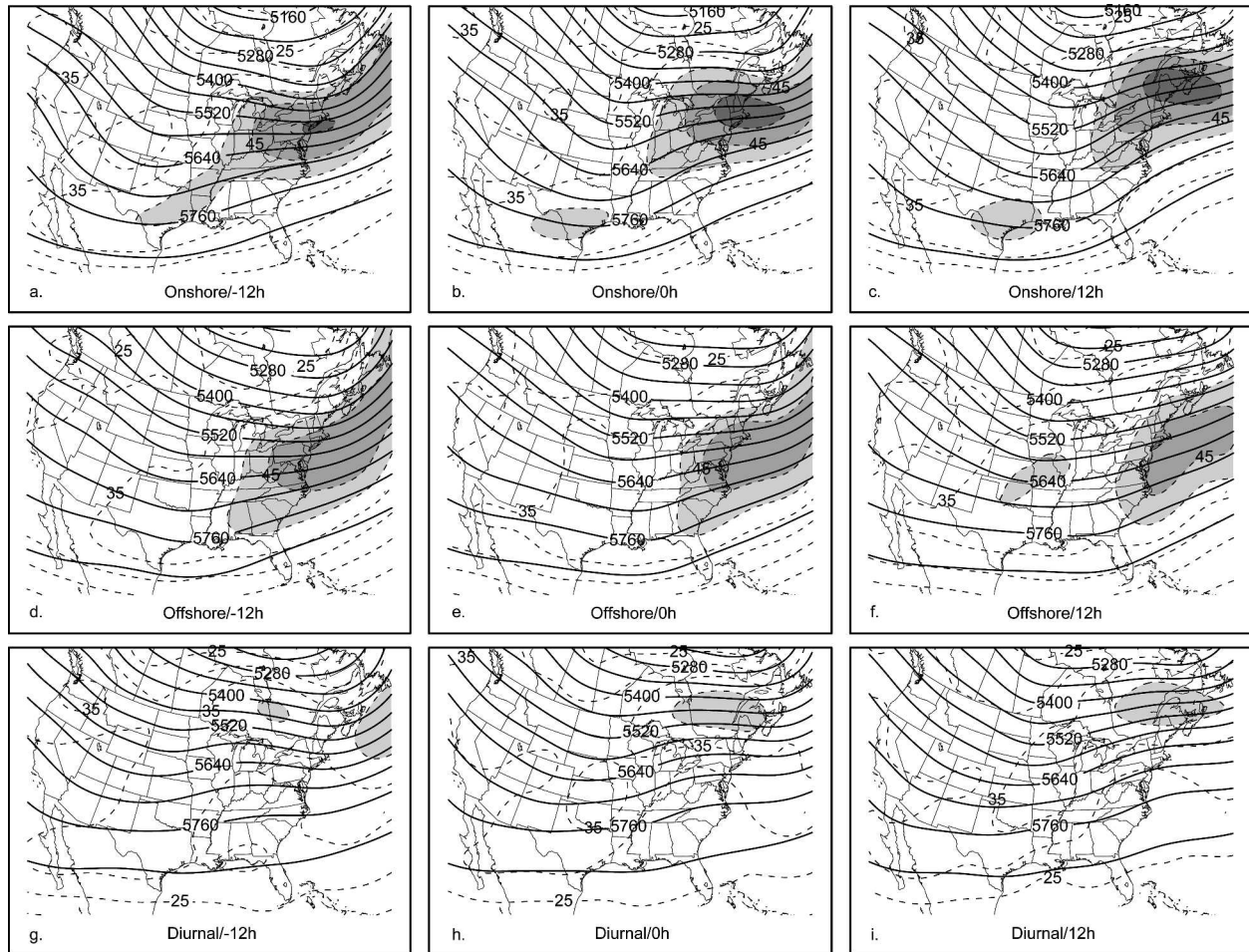


FIG. 16. Composite maps of 500-hPa heights (solid lines labeled in m) and 250-hPa isotachs (dashed lines labeled in m s^{-1} with areas progressively shaded for values over 40 m s^{-1}) for each of three coastal front categories. As in Fig. 12, maps are for 12-h intervals centered at the time of frontogenesis.

- Onshore fronts are associated with surface cyclogenesis or troughing in the Gulf of Mexico, comparatively strong upper-level dynamics, strong warm advection, and onshore flow at low levels along the Southeast coast.
- The significant synoptic features associated with onshore and diurnal coastal fronts in the Carolinas resemble those for New England coastal frontogenesis.
- Offshore fronts are generally accompanied by persistent surface ridging in the Gulf and limited offshore movement of the parent anticyclone. Drier conditions inland over the Southeast and limited low-level warm advection are also characteristic of this type.
- Diurnal fronts are best differentiated by a persistent east–west ridging that accompanies a parent anticyclone centered farther south than in the other two types. Dry conditions inland and very limited warm advection for this type resemble those for the off-

shore case, but for the diurnal fronts the anticyclone center appears to progress eastward and offshore. This type exhibits the weakest upper-level dynamics.

The composite results appear dynamically consistent with frontal theory and with the observed kinematic behavior of coastal fronts. For example, the low-level warm advection, higher relative humidity, an approaching upper trough, and stronger jet dynamics for the onshore case are consistent with regional synoptic-scale ascent and frontogenesis across the Southeast coastal region.

Results of this study strongly suggest that combinations of key features in the composites are useful in forecasting frontal evolution since many of these signals are evident when the front is first identified offshore. It would be interesting to determine if these same key features forecast by operational NWP models can be

used to reliably predict the onset of coastal frontogenesis and to differentiate among the three types. Detailed case studies chosen for their resemblance to or contrast from each category would also be useful in future research.

The present study was restricted to coastal fronts that form offshore. Future research is needed to identify fronts that form slightly inland, as, for example, west of Cape Hatteras. It would also be useful to develop objective methods to document the climatological behavior of coastal fronts and their associated sensible weather after they move inland.

Acknowledgments. We thank forecasters at the National Weather Service Offices throughout the region for helpful guidance and feedback. Special thanks to Chris Bailey for his work developing the composite algorithm and to Gary Lackmann, Lian Xie, Mike Trexler, Scott Kennedy, and Mike Brennan for valuable guidance. Support for this work was provided by NOAA's Collaborative Science Technology and Applied Research (CSTAR) program under Grant NA-07WA0206 and by the NSF Minority Graduate Education program.

REFERENCES

- Austin, J. M., 1941: Favorable conditions for cyclogenesis near the Atlantic coast. *Bull. Amer. Meteor. Soc.*, **22**, 270–272.
- Bailey, C. M., G. Hartfield, G. M. Lackmann, K. Keeter, and W. S. Sharp, 2003: An objective climatology, classification scheme, and assessment of sensible weather impacts for Appalachian cold-air damming. *Wea. Forecasting*, **18**, 641–661.
- Ballentine, R. J., 1980: A numerical investigation of New England coastal frontogenesis. *Mon. Wea. Rev.*, **108**, 1479–1497.
- Barber, D. A., J. M. Davis, and A. J. Riordan, 1984: Spectral analysis of station pressure as an indicator of climatological variations in synoptic-scale activity in the eastern United States. *Mon. Wea. Rev.*, **112**, 333–339.
- Bell, G. D., and L. F. Bosart, 1989: The large-scale atmospheric structure accompanying New England coastal frontogenesis and associated North American east coast cyclogenesis. *Quart. J. Roy. Meteor. Soc.*, **115**, 1133–1146.
- Bosart, L. F., 1975: New England coastal frontogenesis. *Quart. J. Roy. Meteor. Soc.*, **101**, 957–978.
- , 1981: The Presidents' Day snowstorm of 18–19 February 1979: A subsynoptic-scale event. *Mon. Wea. Rev.*, **109**, 1542–1566.
- , C. J. Vaudo, and J. H. Helsdon Jr., 1972: Coastal frontogenesis. *J. Appl. Meteor.*, **11**, 1236–1258.
- Businger, S., W. H. Bauman III, and G. F. Watson, 1991: The development of the Piedmont front and associated outbreak of severe weather on 13 March 1986. *Mon. Wea. Rev.*, **119**, 2224–2251.
- Carson, R. B., 1950: The Gulf Stream front: A cause of stratus on the lower Atlantic coast. *Mon. Wea. Rev.*, **78**, 91–101.
- Chiu, W.-C., 1973: On the atmospheric kinetic energy spectrum and its estimation at some selected stations. *J. Atmos. Sci.*, **30**, 377–391.
- Doyle, J. D., and T. T. Warner, 1990: Mesoscale coastal processes during GALE IOP 2. *Mon. Wea. Rev.*, **118**, 283–308.
- , and —, 1993a: Nonhydrostatic simulations of coastal mesobeta-scale vortices and frontogenesis. *Mon. Wea. Rev.*, **121**, 3371–3392.
- , and —, 1993b: A numerical investigation of coastal frontogenesis and mesoscale cyclogenesis during GALE IOP 2. *Mon. Wea. Rev.*, **121**, 1048–1077.
- Hartmann, D. L., 1974: Time spectral analysis of mid-latitude disturbances. *Mon. Wea. Rev.*, **102**, 348–362.
- Kalnay, E., and Coauthors, 1996: The NCEP/NCAR 40-Year Reanalysis Project. *Bull. Amer. Meteor. Soc.*, **77**, 437–471.
- Lackmann, G. M., L. F. Bosart, and D. Keyser, 1996: Planetary- and synoptic-scale characteristics of explosive wintertime cyclogenesis over the western North Atlantic Ocean. *Mon. Wea. Rev.*, **124**, 2672–2701.
- Marks, F. D., and P. M. Austin, 1979: Effects of the New England coastal front on the distribution of precipitation. *Mon. Wea. Rev.*, **107**, 53–67.
- Nielsen, J. W., 1989: The formation of New England coastal fronts. *Mon. Wea. Rev.*, **117**, 1380–1400.
- , and P. P. Neilley, 1990: The vertical structure of New England coastal fronts. *Mon. Wea. Rev.*, **118**, 1793–1807.
- Olson, D. B., O. B. Brown, and S. R. Emmerson, 1983: Gulf Stream frontal statistics from Florida Straits to Cape Hatteras derived from satellite and historical data. *J. Geophys. Res.*, **88**, 4569–4577.
- Raman, S., N. C. Reddy, and D. S. Niyogi, 1998: Mesoscale analysis of a Carolina coastal front. *Bound.-Layer Meteor.*, **86**, 125–145.
- Riordan, A. J., 1990: Examination of the mesoscale features of the GALE coastal front of 24–25 January 1986. *Mon. Wea. Rev.*, **118**, 258–282.
- , J. T. Anderson, and S. Chiswell, 1995: Small-scale structure of a coastal front as revealed by dual-Doppler radar. *Mon. Wea. Rev.*, **123**, 622–640.
- Sanders, F., 1955: An investigation of the structure and dynamics of an intense surface frontal zone. *J. Meteor.*, **12**, 542–552.
- , and C. A. Doswell III, 1995: A case for detailed surface analysis. *Bull. Amer. Meteor. Soc.*, **76**, 505–521.
- Vescio, M. D., K. Keeter, G. Dial, P. Badgett, and A. J. Riordan, 1993: A low-top weak reflectivity severe weather episode along a thermal/moisture boundary in eastern North Carolina. Preprints, *17th Conf. on Severe Local Storms*, St. Louis, MO, Amer. Meteor. Soc., 628–632.